

# Differential cross-sections measurements for hadrontherapy: 50 MeV/A $^{12}\text{C}$ reactions on H, C, O, Al and $^{nat}\text{Ti}$ targets

C. Divay<sup>1,a</sup>, J. Colin<sup>1</sup>, D. Cussol<sup>1</sup>, Ch. Finck<sup>2</sup>, Y. Karakaya<sup>2</sup>, M. Labalme<sup>1</sup>, M. Rousseau<sup>2</sup>, S. Salvador<sup>1</sup>, and M. Vanstalle<sup>2</sup>

<sup>1</sup> LPC-Caen, ENSICAEN, Université de Caen Normandie, CNRS/IN2P3, Caen, France

<sup>2</sup> Institut Pluridisciplinaire Hubert Curien, Strasbourg, France

**Abstract.** In order to keep the benefits of a carbon treatment, the dose and biological effects induced by secondary fragments must be taken into account when simulating the treatment plan. These Monte-Carlo simulations codes are done using nuclear models that are constrained by experimental data. It is hence necessary to have precise measurements of the production rates of these fragments all along the beam path and for its whole energy range. In this context, a series of experiments aiming to measure the double differential fragmentation cross-sections of carbon on thin targets of medical interest has been started by our collaboration. In March 2015, an experiment was performed with a 50 MeV/nucleon  $^{12}\text{C}$  beam at GANIL. During this experiment, energy and angular differential cross-section distributions on H, C, O, Al and  $^{nat}\text{Ti}$  have been measured. In the following, the experimental set-up and analysis process are briefly described and some experimental results are presented. Comparisons between several exit channel models from PHITS and GEANT4 show great discrepancies with the experimental data. Finally, the homemade SLIPIE model is briefly presented and preliminary results are compared to the data with a promising outcome.

## 1. Introduction

Hadrontherapy presents several benefits over conventional radiotherapy. It takes advantage of the energy deposition process of the charged ions by the presence of the Bragg peak to allow for more conformal dose deposition distributions [1]. It can be performed using protons or heavier ions, reducing in this case the lateral scattering. But the most important benefit resides in the biological effects. In fact, the Relative Biological Effectiveness (RBE, the efficiency for a radiation to kill a tumor cell) can be two to three times greater for  $^{12}\text{C}$  than for protons or photons.

However, accelerated ions going through matter are subject to nuclear interactions, having for first consequence to decrease the number of beam particles along the penetration path [2]. Moreover, secondary fragments created by these reactions lead to a delocalization of the dose in the surrounding healthy tissues and to a mixed irradiation field of heterogeneous RBE values that will modify the biological dose distribution. These effects are still not well known and no nuclear model in the available generic simulation codes is able to accurately reproduce the fragment production.

In order to provide data for the improvement of the simulation codes, our collaboration performed two experiments at 95 MeV/nucleon in 2011 [3] and 2013 [4] and one at 50 MeV/nucleon in 2015 at the Grand Accélérateur National d'Ions Lourds (GANIL) in Caen, France. The aim of these experiments was to measure the energy and angular differential fragmentation cross-sections of  $^{12}\text{C}$  ions on thin targets of C,  $\text{CH}_2$ , Al,  $\text{Al}_2\text{O}_3$  and  $^{nat}\text{Ti}$ . From the measurements on the C and  $\text{CH}_2$

targets, we were able to extract the cross-sections of  $^{12}\text{C}$  on hydrogen and from the Al and  $\text{Al}_2\text{O}_3$  targets, the cross-sections on oxygen. Assuming that the cross-sections at forward angles are dominated by the projectile fragmentation, the cross-sections for  $^{nat}\text{Ti}$  ( $Z=22$ ) should be very close to those of  $^{40}\text{Ca}$  ( $Z=20$ ). We then have access to the cross-sections for four elements that constitute 95% of the human body, H, C, O and Ca.

The 50 MeV/nucleon experiment, the data analysis and the results are detailed in a paper submitted to PRC [5]. In the following, the experiment will be briefly presented, as well as differential and integrated cross-sections. Then, data will be compared to several models included in GEANT4 [6] and PHITS [7]. Finally, the model called SLIPIE [8] will be presented and preliminary results will be shown.

## 2. The 50 MeV/nucleon experiment

The experiment took place at GANIL with a 50 MeV/nucleon  $^{12}\text{C}$  beam. All the targets used had an area density of about  $0.05\text{ g}\cdot\text{cm}^{-2}$ . The fragment detection setup consisted of five telescopes, each composed of three layers: a thin and a thick silicon diode and a thick CsI scintillating crystal coupled to a PMT. The setup was located in a vacuum reaction chamber. A detailed description of the experiment setup can be found in [5].

The identification process was performed using the  $\Delta E - E$  method. Some misidentification and pile-up events in the detectors have been removed thanks to the use of a Pulse Shape Analysis of the CsI signal. The method describing in details the different analysis processes can be found in [5,9].

<sup>a</sup> e-mail: divay@lpc-caen.in2p3.fr

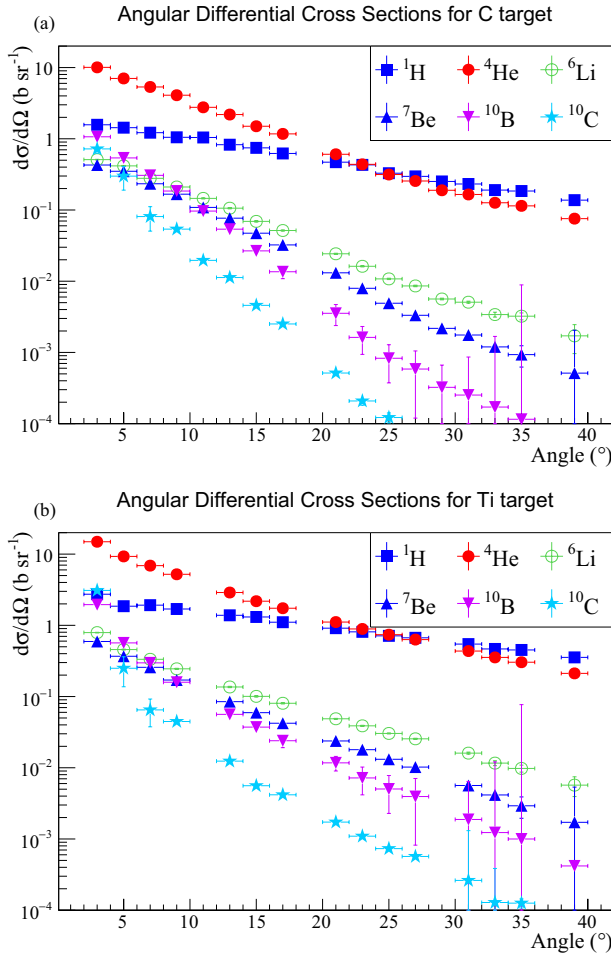


**Figure 1.** Angular differential cross-sections distributions of 6 isotopes from Z=1 to Z=6 for the carbon (a) and titanium (b) targets.

The angular cross-sections were calculated using the formula:

$$\frac{d\sigma}{d\Omega}({}^A_ZX) = \frac{N({}^A_ZX) \times A_{\text{target}}}{N({}^{12}\text{C}) \times \Omega \times (\rho \times th)_{\text{target}} \times \mathcal{N}_A}, \quad (1)$$

where  $N({}^A_ZX)$  is the number of fragments of mass A and charge Z detected,  $N({}^{12}\text{C})$  is the number of beam ions measured by the beam monitor,  $A_{\text{target}}$  is the number of mass of the target,  $\Omega$  is the solid angle covered by the detector,  $(\rho \times th)_{\text{target}}$  is the area density of the target and  $\mathcal{N}_A$  is the Avogadro number.

All the double differential cross-sections were measured for every isotope from proton to  ${}^{12}\text{C}$ , every target and angles ranging from  $3^\circ$  to  $39^\circ$ . In the following section, the results will be quickly presented in form of angular distributions. These distributions were also integrated to calculate the production cross-sections of each isotope for comparison with a previous experiment at 95 MeV/nucleon [3].

### 3. Experimental results

#### 3.1. Differential cross-sections

An example of angular distributions is shown in Fig. 1 for (a) the carbon and (b) the titanium target. The distributions displayed are obtained for various isotopes from  ${}^1\text{H}$  to

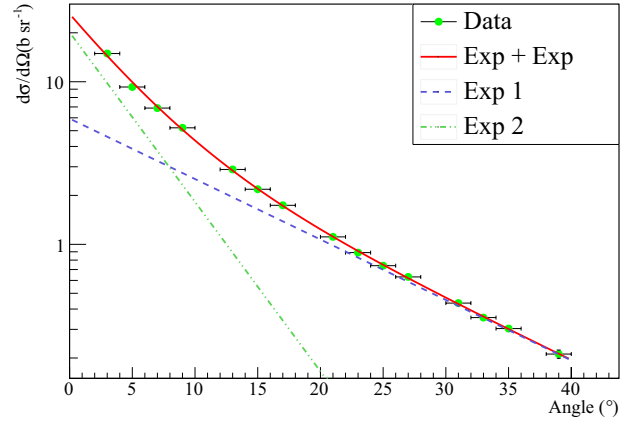


**Figure 2.** Fitted function over the angular distribution of  ${}^4\text{He}$  production for titanium target. The two individual exponential functions are plotted in dashed and dash-dotted lines and the sum is depicted in a continuous red line.

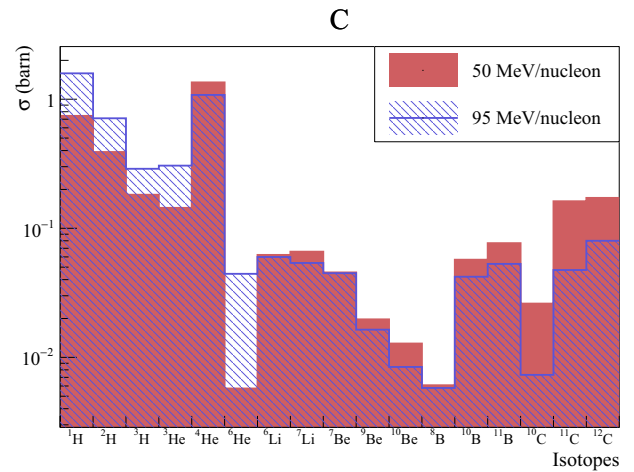


**Figure 3.** Production cross-section per isotope for the 50 MeV/nucleon (plain red) and the 95 MeV/nucleon (hashed blue) experiment.

${}^{10}\text{C}$ . A clear dominance of light isotopes (mostly protons and  $\alpha$  particles) is observed over the whole angular range. Up to  $25^\circ$ , the  ${}^4\text{He}$  production dominates the proton production. Overall, it can be seen that the higher the mass of the fragment, the more forward peaked the angular distribution. As seen in Fig. 1(b) for the titanium target, the cross-sections also increase with the target mass. The shape of the distributions is also different: most of the distributions present an emphasized peaked behavior at very forward angles.

#### 3.2. Production cross-sections

The 95 MeV/nucleon experiments [4] showed that the best way to reproduce the shape of the angular distributions was by using a sum of a Gaussian and two exponential functions. But the lack of a  $0^\circ$  measurement for our experiment makes it impossible to constrain the three functions between  $0^\circ$  and  $3^\circ$ . The choice was made to use the sum of two exponential functions to reproduce the distributions for all fragments and all targets. An example of such function is shown in Fig. 2 for the  ${}^4\text{He}$  production on the Ti target.

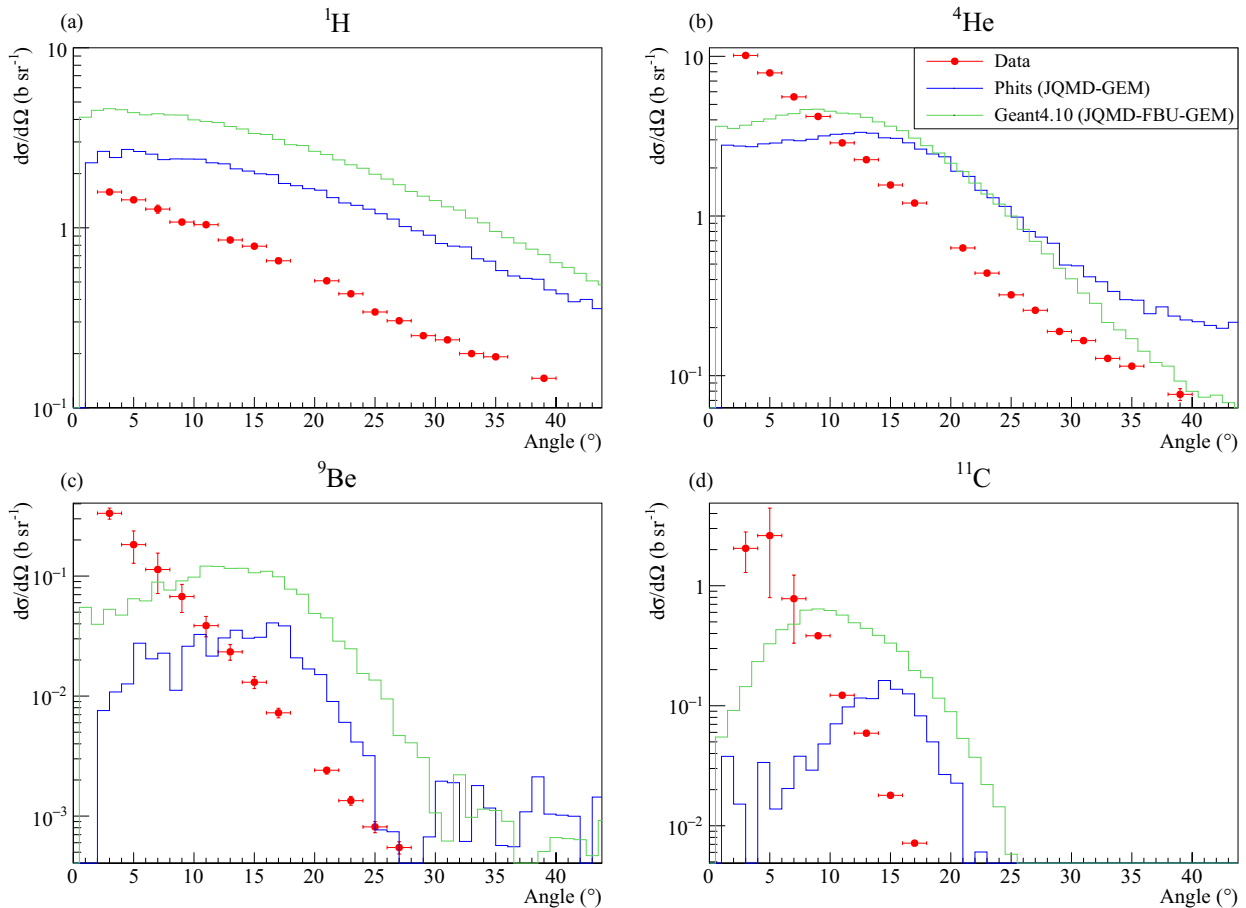


**Figure 4.** Comparison between the experimental data and simulations of angular distributions for the production of (a) protons, (b)  $\alpha$ , (c)  ${}^9\text{Be}$  and (d)  ${}^{11}\text{C}$ . Data are represented in red dots while the defaults models of Phits and Geant are represented in blue and green lines, respectively.

By integrating the fitted functions over the whole angular range, one can obtain the production cross-section of a given isotope. The results are gathered in Fig. 3 and compared to the production cross-sections obtained for the 95 MeV/nucleon experiment. The fragment production is dominated by light particles emission, especially  $\alpha$  and protons. The light fragments production is clearly lower at 50 MeV/nucleon than at 95 MeV/nucleon, with the exception of the  $\alpha$  particle production that presents a slight increase, as the  $3\text{-}\alpha$  fragmentation channel of  ${}^{12}\text{C}$  should be favored when the beam energy decreases. It also appears that the production of the heaviest isotopes (boron and carbon) is higher at 50 MeV/nucleon.

## 4. Monte-Carlo simulations

In the following section, the angular distributions obtained with this experiment will be compared with different models included in the Monte-Carlo codes GEANT4 and PHITS. In particular, the differences between exit channel models will be studied. In a second time, the homemade model called SLIPIE [8] will be briefly presented and tested.

### 4.1. GEANT4 and PHITS

For this study, we used GEANT4 version 10.02-p01. The JQMD [10,11] entrance channel model was used as it was the only model in GEANT4 whose energy range included

50 MeV/nucleon. The default exit channel is a combination between the Fermi Break-Up model (FBU) [10] and the Generalized Evaporation Model (GEM) [10,12], but GEANT4 proposes to deactivate one or the other.

The version 2.82 of PHITS was used with JQMD as entrance channel model. The code proposes the GEM exit channel model as default but three other are available: the Statistical Decay Model (SDM), the Dresden model (DRES) and the Statistical Multifragmentation Model (SMM).

Figure 4 presents the angular distributions for protons,  $\alpha$  particles,  ${}^9\text{Be}$  and  ${}^{11}\text{C}$  as produced by the default settings of GEANT4 and PHITS compared to the measured data. It is clear that the two simulations present similar results. The proton production [Fig. 4(a)] is overestimated, even though the shape of the distributions is similar to the experimental data. The production of  $\alpha$  particles is shown in Fig. 4(b). The shape of the distributions generated by the two codes both present a peak around  $15^\circ$  that was not observed experimentally. This peaked behavior is also observed and emphasized for all heavier isotopes and implies a great underestimation of the production at low angles, as seen in Fig. 4(c) and (d). The same behavior has also been observed at 95 MeV/nucleon.

The differences between three exit channels in GEANT4 are shown in Fig. 5. The shape of the proton angular distribution stays the same and the cross-sections values are separated by a factor of two at most. The  $\alpha$

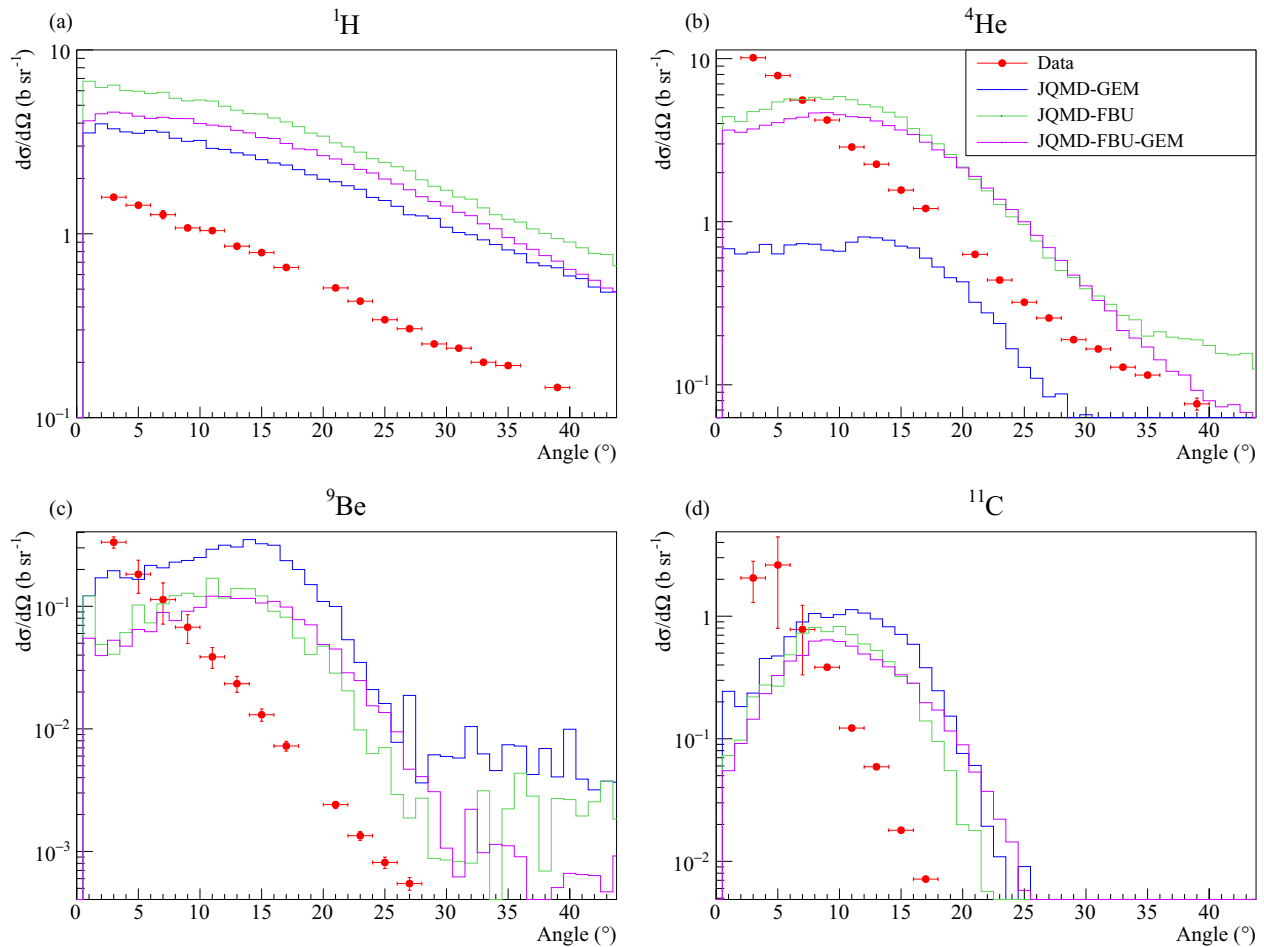


**Figure 5.** Comparison between the experimental data and a Geant4 simulation of angular distributions for the production of (a) protons, (b)  $\alpha$ , (c)  ${}^9\text{Be}$  and (d)  ${}^{11}\text{C}$ . Data are represented in red dots, results with FBU, GEM and FBU+GEM are represented in green, blue and purple lines, respectively.

particle production is impacted by nearly a factor of ten when deactivating the FBU model. However, it does not seem that deactivating the GEM model has a great impact on the fragment production. The three models present a similar behavior for the production of heavier isotopes [Fig. 5(c) and (d)]. The shape of the distributions are comparable and the cross-sections values are separated by a factor of two to three.

In the same way than with GEANT4, the proton production is not significantly affected by the exit channel in PHITS. In Fig. 6(a), only the Dresden model shows a different shape, with the presence of a peak around 15°, while the cross-sections values are separated by a factor of two to three at most. For the  $\alpha$  particle production shown in Fig. 6(b), the same behavior is observed. The GEM, SDM and SMM models present very similar results while the DRES model shows important differences. For the  ${}^9\text{Be}$  production [Fig. 6(c)], all the models present the same shape, but the SDM and DRES models show cross-sections significantly lower and close to zero before 5°. In Fig. 6(d), it can be seen that the  ${}^{11}\text{C}$  production is very similar between all the models.

It is clear that the exit channel model can have a great impact on the results of a simulation, but it cannot be said that one model performs better than the other. In GEANT4, it seems that the FBU models must be activated in order to give more realistic results as concluded before

in [13, 14]. In PHITS, it was shown that the Dresden model gives the worst results. Nevertheless, none of the models available to the public are able to reproduce the data at 50 MeV/nucleon in a satisfactory manner.

The same conclusion was drawn from the 95 MeV/nucleon and this is why our collaboration has developed a new model called SLIPIE.

## 4.2. SLIPIE

The SLIPIE model was developed by J. Dudouet and D. Durand in our laboratory and has been described in [8]. It is based on a simple “participant-spectator” geometrical approach where only the nucleons from the overlap region of the two nuclei are participating to the reaction. The participant nucleons from the two nuclei become a hot source of emission called the “mid-rapidity” emission due to the wide velocity distribution of the nucleons. The remaining “spectator” nucleons from the projectile (target) become the quasiprojectile (quasitarget).

This model features only four free parameters that were adjusted to best reproduce the 95 MeV/nucleon data. The entry channel is described as semimicroscopic, since it considers the spatial and momentum distributions of the nucleons in the nuclei as well as macroscopic quantities like the excitation energies of the fragments. The exit channel is a homemade Fermi break-up model.

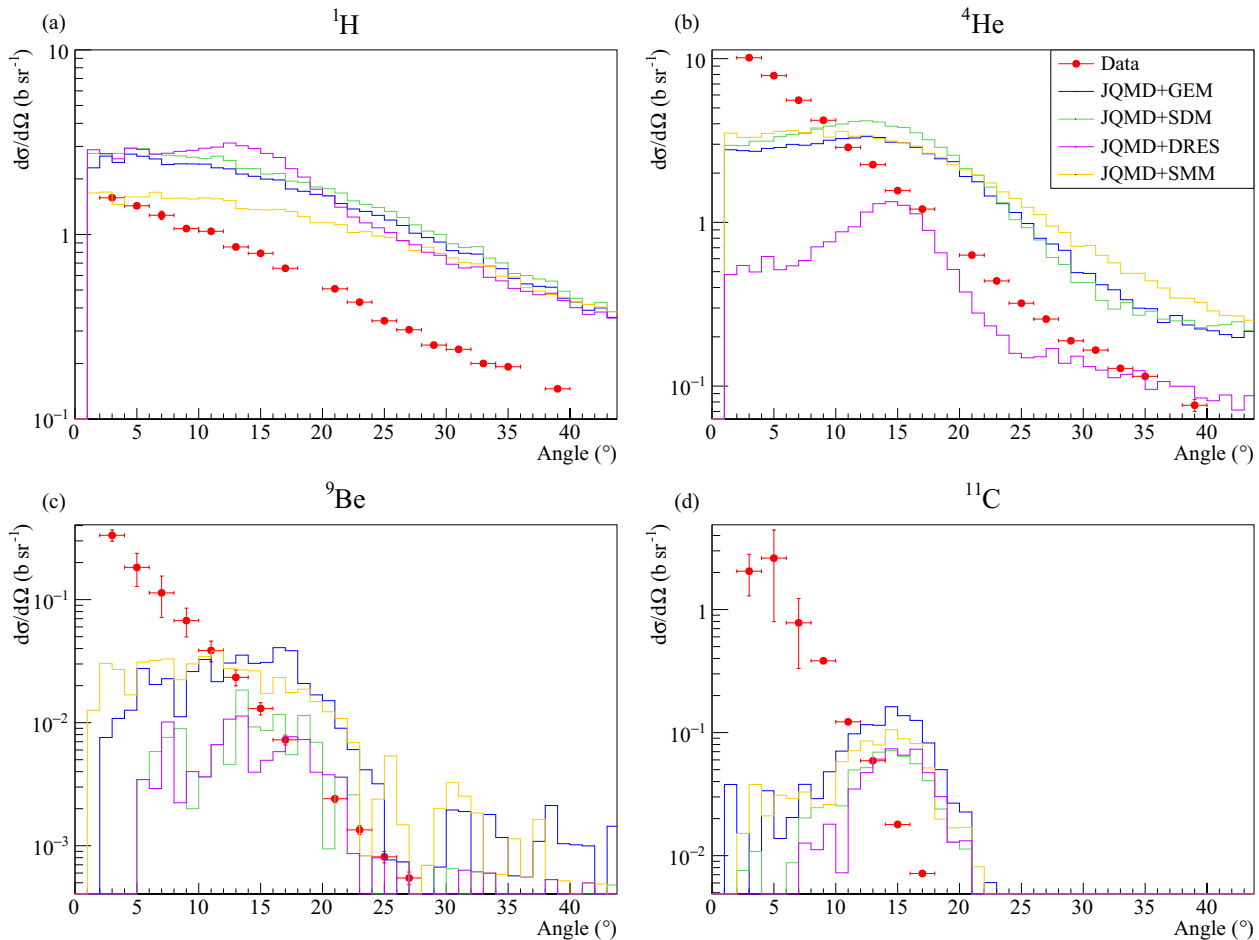


**Figure 6.** Comparison between the experimental data and simulations of angular distributions for the production of (a) protons, (b)  $\alpha$ , (c)  ${}^9\text{Be}$  and (d)  ${}^{11}\text{C}$ . Data are represented in red dots while the different exit channels of Phits are represented in blue, green, purple and orange lines.

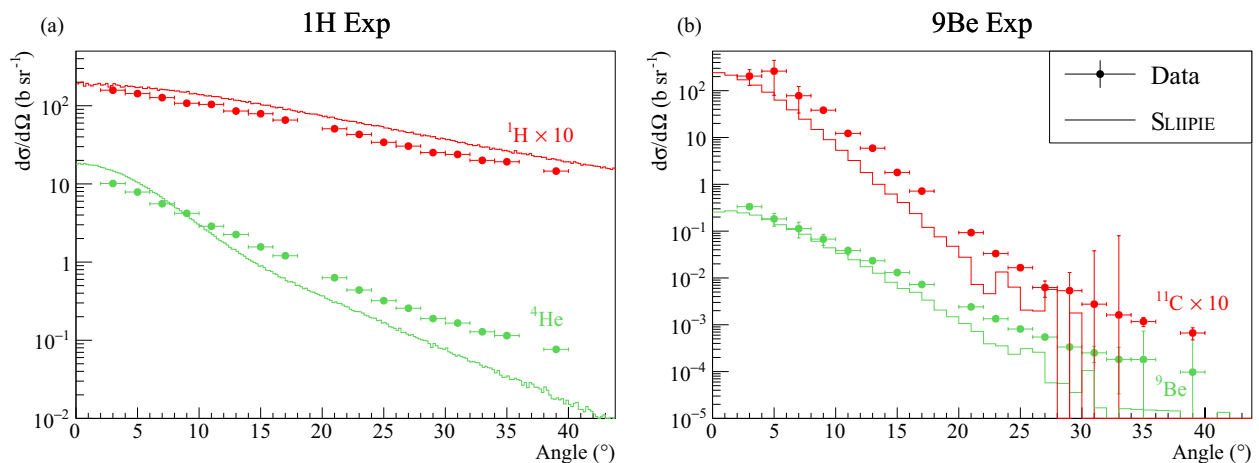


**Figure 7.** Comparison between the experimental data and simulations of angular distributions for the production of (a) protons and  $\alpha$  particles, and (b)  ${}^9\text{Be}$  and  ${}^{11}\text{C}$ . Data are represented in dots and the results of SLIPIE are represented by lines. The isotope name is given aside each distribution.

Figure 7 shows the results of a 50 MeV/nucleon simulation using the default settings of SLIPIE defined to best reproduce the 95 MeV/nucleon data [8]. The agreement is better than with any of the previously tested models. The proton production is overestimated by about 50% on all the angular range while the distributions for  $\alpha$  particles are a little too peaked at forward angles. This results in an overestimation of the cross-sections

at very low angles and an underestimation after about  $10^\circ$ . The cross-sections for the heavier fragments in Fig. 7(b) is a little underestimated, but the shape of the distributions is very close to the experimental data.

In order to obtain the optimal results from this code, a systematic study is ongoing to find the most suited set of parameters for this energy.

## 5. Conclusion

Fragment production measurements of a 50 MeV/nucleon  $^{12}\text{C}$  beam have been performed for 17 different angles and five different targets of medical interest. This led in obtaining the double differential cross-sections in angle and energy of  $^{12}\text{C}$  on hydrogen, carbon, oxygen, aluminum and titanium between  $3^\circ$  and  $39^\circ$  for all isotopes from protons to  $^{12}\text{C}$ .

The production is dominated by light fragments, especially protons and  $\alpha$  particles. Compared to the 95 MeV/nucleon experiment, it has been shown that the production of heavy fragments and  $\alpha$  particles has increased while the production of lighter fragments has decreased.

A “benchmark” of different models available in GEANT4 and PHITS has shown great discrepancies between the data and the simulation results. While the exit channel showed a great impact on the results of the simulation, it cannot cover the flaws inherent to the entrance channel model. The SLIPIE model, developed and adjusted for the 95 MeV/nucleon data has proven to be better at reproducing these low energy data.

By combining these measurements with those from the 95 MeV/nucleon  $^{12}\text{C}$  beam experiment, the last 2 cm of the  $^{12}\text{C}$  range in the body during a treatment are covered. These sets of data (angular and energy distributions for each target) are available for free access on the website <http://hadrontherapy-data.in2p3.fr>.

To complete these data up to the maximum energy used for treatment (e.g. 400 MeV/nucleon), new measurements are planned in the future ARCADE research and treatment center in Caen.

## References

- [1] D. Schardt et al., Rev. Modern Phys. **82** (2010)
- [2] A.S. Goldhaber, Ann. Rev. of Nucl. Part. Sci. **28**, 161 (1978)
- [3] J. Dudouet et al., Physical Review C **88**, 024606 (2013), <http://hal.in2p3.fr/in2p3-00829487>
- [4] J. Dudouet et al., Physical Review C **89**, 064615 (2014), <http://hal.in2p3.fr/in2p3-01017198>
- [5] C. Divay et al., Physical Review C **95**(4), 044602 (2017)
- [6] S. Agostinelli et al., Nucl. Instrum. Methods Phys. Res. A **506**, 250 (2003)
- [7] T. Ogawa et al., J. Nucl. Sci. Technol. **50**(9), 913 (2013)
- [8] J. Dudouet, D. Durand, Physical Review C **94**, 014616 (2016)
- [9] J. Dudouet et al., Nucl. Instrum. Methods Phys. Res. A **715**, 98 (2013), <http://hal.in2p3.fr/in2p3-00806234>
- [10] *Geant4 physics reference manual* (2015)
- [11] T. Koi, Proceedings, Joint International Conference on Supercomputing in Nuclear Applications and Monte Carlo, Tokyo, Japan (**SNA+MC2010**) (2010)
- [12] S. Furihata et al., Nucl. Instrum. Methods Phys. Res. B **171**, 251 (2000)
- [13] J. Dudouet et al., Physical Review C **89**, 054616 (2014)
- [14] T.T. Böhlen et al., Phys. Med. Biol. **55**, 5833 (2010)